Available online at www.sciencedirect.com

ScienceDirect

Physics Procedia 17 (2011) 30–39

Physics Procedia

Physics of Fundamental Symmetries and Interactions – PSI2010

# *R*- and *N*-correlation coefficients in neutron decay: Search for scalar and tensor couplings in weak interactions

K. Bodek[a,*], G. Ban[b], A. Białek[c], P. Gorel[b,d,a], K. Kirch[d,e], St. Kistryn[a], A. Kozela[c], M. Kuźniak[a,d], O. Naviliat-Cuncic[b], N. Severijns[f], E. Stephan[g], J. Zejma[a]

[a] *M Smoluchowski Institute of Physics, Jagiellonian University, Cracow, Poland*
[b] *LPC-Caen, ENSICAEN, Universit de Caen Basse-Normandie, CNRS/IN2P3-ENSI, Caen, France*
[c] *H. Niewodniczański Institute of Nuclear Physics, Polish Academy of Sciences, Cracow, Poland*
[d] *Paul Scherrer Institute, Villigen, Switzerland*
[e] *Swiss Federal Institute of Technology, Zurich, Switzerland*
[f] *Instituut voor Kern- en Stralingsfysica, Katholieke Universiteit, Leuven, Belgium*
[g] *Institut of Physics, University of Silesia, Katowice, Poland*

**Abstract**

The decay correlation coefficients $R$ and $N$ have been measured with the aim to search for scalar and tensor admixtures to the V-A interaction dominating in the neutron decay. Both $R$ and $N$ are accessible in the two transverse components of the electron polarization which was analyzed with Mott scattering from lead nuclei. The analysis of data collected in four runs is in its final stage giving the preliminary results consistent with the Standard Model: $R = 0.005 \pm 0.013(\text{stat.}) \pm 0.005(\text{syst.})$ and $N = 0.064 \pm 0.012(\text{stat.}) \pm 0.004(\text{syst.})$, respectively. A possible future experiment leading to an accuracy improved by at least an order of magnitude and more systematic investigation of the electron spin related correlation coefficients is discussed as well.

*Keywords:* Standard Model, scalar and tensor interactions, cold neutrons, neutron decay, Mott scattering
*PACS:* 24.10.+y, 23.40.Dw, 24.70.+s, 11.30.+s

## 1. Introduction

The Standard Model (SM) predictions of time-reversal violation for weak decays of systems built up of $u$ and $d$ quarks are by 7 to 10 orders of magnitude lower than the experimental accuracies attainable at present. It is a general presumption that time-reversal phenomena are caused by a tiny admixture of exotic interaction terms. Therefore, weak decays provide a favorable testing ground in a search for such feeble forces. Our experiment seeks for small deviations from the SM in two observables that have never before been addressed experimentally in free neutron decay. The first of these, the $R$-correlation coefficient, is proportional to the electron polarization component perpendicular to the plane spanned by the spin of the decaying neutron and the electron momentum. Its non-zero value (corrected for the electromagnetic effects) would signal a violation of time-reversal symmetry and thus the existence of physics beyond the Standard Model. The second observable, the $N$-correlation coefficient, is given by the transverse electron

*Corresponding author
*Email address:* kazimierz.bodek@uj.edu.pl (K. Bodek)


doi:10.1016/j.phpro.2011.06.014

polarization component within the above mentioned plane. Within the SM its value is significantly different from zero and it scales with the decay asymmetry parameter $A$. The measurement of $N$, both probes the SM and serves as an important systematic check of the experimental apparatus and the applied analysis procedure with respect to the $R$-correlation measurement. The $N$- and $R$-correlation coefficients are sensitive to either real or imaginary parts of the same linear combination of the scalar and tensor interaction coupling constants, respectively. Experimental determination of the $N$ and $R$ coefficients will help to further constrain possible contributions of these exotic couplings.

## 2. Experiment and data analysis

The experiment has been carried out on the polarized cold neutron beam facility FUNSPIN of the SINQ spallation source at the Paul Scherrer Institute, Villigen, Switzerland. The transverse polarization of electrons from the neutron decay was analyzed in the Mott scattering from lead nuclei. A beam of polarized cold neutrons with a total intensity of about $10^{10}$ s$^{-1}$ was transported in pure helium gas in front of two detection systems each consisting of a multiwire proportional chamber (MWPC), a scattering Pb foil and a plastic scintillator hodoscope as sketched in Fig. 1. Electron

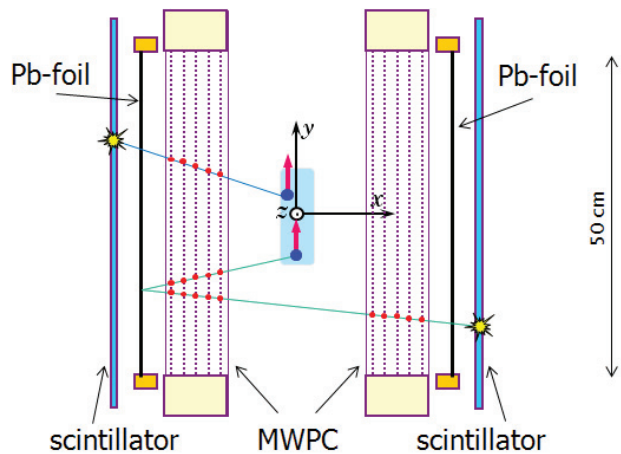


Figure 1: Sketch of the Mott polarimeter setup. A sample projection of an electron single track and a V-track event are indicated.

tracks were used to reconstruct the electron momenta and identify the scattering vertices ("V-track events") – a powerful tool for background reduction. The detailed description of the experimental apparatus and applied techniques has been published elsewhere [1] an will not be repeated here. Instead, we will briefly present new calibrations helping to better assess systematic errors due to multiple scattering effects in the Mott target. Moreover, an alternative method of extraction of both $N$ and $R$ coefficients from independent fits to the experimental data will be discussed, too.

One of the dominant systematic uncertainties is connected with the effective analyzing power of the Mott polarimeter. This quantity is mitigated by multiple Coulomb scattering of electrons which take place mainly in lead and depolarize electrons prior to Mott scattering. The magnitude of that depolarization depends, in turn, on energy and target thickness and is accounted for in the data analysis with the help of the Monte Carlo transport code. The reliability of the resulting effective analyzing power and its final uncertainty depends on the quality of the model used for electron scattering on atoms and on the accuracy of the target thickness. Both these issues were addressed in the calibration procedure described in the following sections.

The evaporation technique used for the production of a thin lead layer did not guarantee high uniformity. This is why in the former analysis we assigned a relatively large systematic uncertainty to the effective analyzing power. In order to improve that we measured with the X-ray induced fluorescence technique the mass distribution of both targets used in the experiment. The achieved relative accuracy was $\approx$1% and the absolute normalization was better than 0.5 $\mu$g/cm$^2$. The parameters of the Geant4 based Monte Carlo transport code evaluating the effective analyzing power as a function of electron incident energy, incident scattering angles and target thickness were calibrated by comparing the calculations with three sets of experimental data [2, 3] (i) Au, $E$ = 120 keV, $\sigma$ = 135 $\mu$g/cm$^2$, (ii) Au, $E$ = 120

keV, $\sigma = 222\ \mu g/cm^2$ and (iii) Pb, $E = 14$ MeV, $\sigma = 34$ mg/cm$^2$. The achieved agreement is on the level of 1–2% and improves with increasing energy and target thickness. One can conservatively conclude that an overall uncertainty of the effective analyzing power is on the 3% level.

The former data analysis [4] was limited to the events with Mott scattering vertices coinciding in two projections. The events with a weaker signature (only one vertex, scattering plane parallel to either anode or cathode wires) were left over as supposed to reveal this higher background. Fortunately, this kind of events reveals higher background contribution mainly outside the applied cuts as can be seen in Fig. 2(a). A subset of the single vertex events, those in the

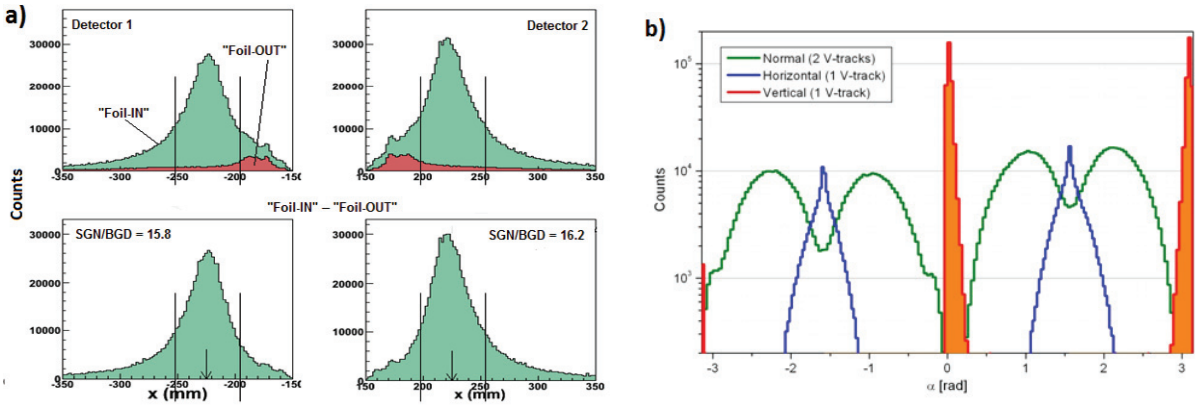


Figure 2: a) Vertex position distribution of the reconstructed "vertical" V-track events. Arrows indicate the nominal target position. "Foil-IN", "Foil-OUT" and subtracted distributions are shown. Vertical solid lines indicate the ranges of events accepted to further analysis. b) Population of the angle $\alpha$ with Mott-scattering events with different signatures: V-tracks seen in two projections (green), V-tracks seen in the horizontal plane (blue), V-tracks seen only in the vertical plane (red).

plane parallel to the neutron polarization (called "vertical") are especially valuable for extraction of the $R$ correlation coefficient. The events in the plane perpendicular to the neutron polarization direction (called "horizontal") improve the statistics of the data relevant for the extraction of the $N$ correlation coefficient. Fig. 2(b) presents the population of $\alpha$ – the angle between electron scattering and neutron decay planes with the latter being spanned by the neutron spin and electron momentum. A pronounced and asymmetric grouping of the "vertical" events around $\alpha = 0, \pi$ is an artefact caused by the neutron spin guiding magnetic field together with the limited double-track resolution around those angles. It has a negligible impact on the final results.

The neutron beam polarization averaged over the fiducial volume was deduced from the angular distribution of the spin UP/DOWN asymmetry $\mathcal{E}$ of the decay electrons using the precisely known [5] beta decay asymmetry parameter $A = -0.1173 \pm 0.0013$:

$$\mathcal{E}(\beta,\gamma) = \frac{N^+(\beta,\gamma) - N^-(\beta,\gamma)}{N^+(\beta,\gamma) + N^-(\beta,\gamma)} = PA\beta\cos(\gamma), \tag{1}$$

where $N^\pm$ are experimental, background corrected counts of single tracks (electrons which passed Pb foil without Mott scattering), sorted in 4 bins of the electron velocity $\beta$ and 15 bins of the electron emission angle $\gamma$ with respect to the neutron polarization direction. The sign in superscripts reflects the direction of the beam polarization $P$. Fig. 3(a) shows the fit to the angular distribution of $\mathcal{E}$ deduced from the data collected in the 2007 data taking period.

The values of the $N$ and $R$ correlation coefficients were extracted with a two parameter fit to the neutron spin UP/DOWN asymmetry defined as:

$$\mathcal{A}(\alpha) = \frac{n^+(\alpha) - n^-(\alpha)}{n^+(\alpha) + n^-(\alpha)} = A\,P\beta(\alpha)\mathcal{F}(\alpha) + P\mathcal{S}(\alpha)\left[N\,\mathcal{G}(\alpha) + R\beta(\alpha)\mathcal{H}(\alpha)\right], \tag{2}$$

where $n^\pm$ represent background-corrected experimental numbers of counts of V-track events, sorted in 12 bins of $\alpha$. The kinematical factors $\mathcal{F}(\alpha)$, $\mathcal{G}(\alpha)$ and $\mathcal{H}(\alpha)$ represent the average values of the quantities $\hat{\mathbf{J}}\cdot\hat{\mathbf{p}}_e$, $\hat{\mathbf{J}}\cdot\hat{\boldsymbol{\sigma}}$ and $\hat{\boldsymbol{\sigma}}\cdot(\hat{\mathbf{p}}_e\times\hat{\mathbf{J}})$, respectively. The unit vectors $\hat{\mathbf{J}}$ and $\hat{\mathbf{p}}_e$ are respectively parallel to the neutron polarization and the electron momentum

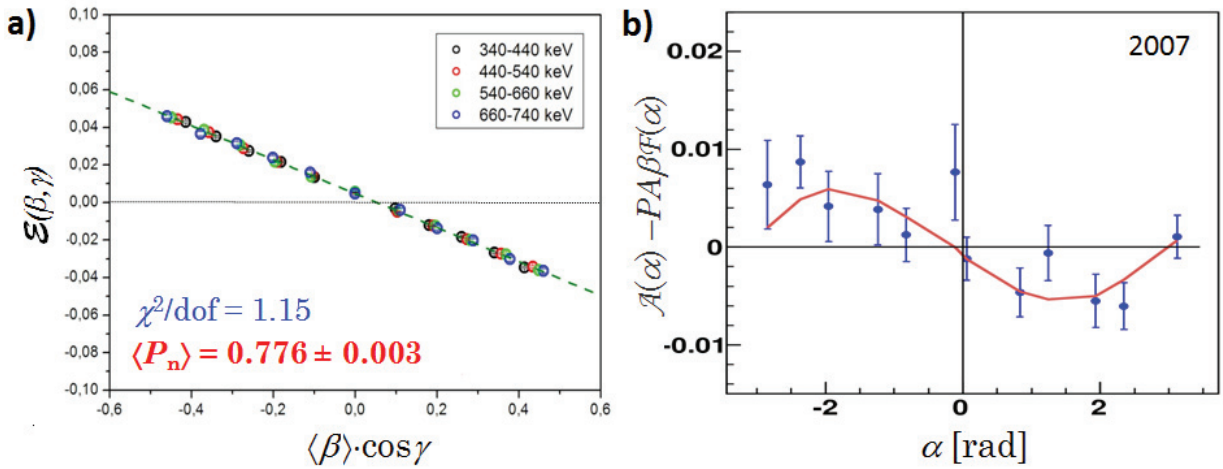


Figure 3: a) Angular distribution of the asymmetry evaluated according to Eq. (1). b) $\alpha$ distribution of the asymmetry evaluated according to Eq. (2) from the Mott scattering events. Both distributions were evaluated from data collected in the run 2007.

while $\hat{\sigma}$ is perpendicular to the Mott scattering plane (electron spin sensing direction). $\mathcal{S}$ is the effective analyzing power of the electron Mott scattering, known in the literature as "Sherman function". The term $P\beta A\mathcal{F}$ accounts for the $\beta$-decay asymmetry induced nonuniform illumination of the Mott foil. Since the $\beta$ and $\mathcal{F}$ are known precisely from event-by-event averaging, the uncertainty of this term is dominated by the error of the average beam polarization $P$. Figure 3(b) shows the $\alpha$ distribution of the above asymmetry.

It turns out that two alternative asymmetries, called here "super-ratios" $\mathcal{N}(\alpha)$ and $\mathcal{R}(\alpha)$, allow for an independent extraction of both $N$ and $R$. They make use of the approximate symmetry of the detecting system with respect to the transformation $\alpha \to -\alpha$. Expanding in small parameters $N$ and $R$ and keeping only first order terms one arrives at:

$$\mathcal{N}(|\alpha|) = \frac{\sqrt{n^+(+\alpha)n^-(-\alpha)} - \sqrt{n^+(-\alpha)n^-(+\alpha)}}{\sqrt{n^+(+\alpha)n^-(-\alpha)} + \sqrt{n^+(-\alpha)n^-(+\alpha)}} = N\frac{P\mathcal{S}(|\alpha|)\mathcal{G}(|\alpha|)}{\beta(|\alpha|)\left[1 - A^2P^2\beta^2(|\alpha|)\mathcal{F}^2(|\alpha|)\right]}, \tag{3}$$

$$\mathcal{R}(|\alpha|) = \frac{\sqrt{n^+(+\alpha)n^+(-\alpha)} - \sqrt{n^-(+\alpha)n^-(-\alpha)}}{\sqrt{n^+(+\alpha)n^+(-\alpha)} + \sqrt{n^-(+\alpha)n^-(-\alpha)}} = A\,P\beta(|\alpha|)\mathcal{F}(|\alpha|) + R\,P\beta(|\alpha|)\mathcal{S}(|\alpha|)\mathcal{H}(|\alpha|). \tag{4}$$

Both double and single vertex events were reanalyzed according to Eqns. (3,4) and taking into account the new calibrated effective Sherman function. Table 1 is the updated version of Table 2 from Ref. [4]. For clarity, the columns entitled as $d$ ($\mu$m), $\bar{E}_K$(keV) and $N_{\mathrm{SM}}\times10^3$ are omitted. At first sight, both approaches give consistent results.

Table 1: Summary of the results obtained in all data collection periods. Statistical and systematical uncertainties follow the experimental values. V and VV stay for single and double vertex event signature, respectively, $\sum(n^+{+}n^-)$ represents the total, background corrected number of Mott-scattered events.

| Run | Sign. | $\sum(n^+{+}n^-)$ | $P\times10^2$ | $N\times10^3$(Eq. 2) | $N\times10^3$ (Eq. 3) | $R\times10^3$(Eq. 2) | $R\times10^3$(Eq. 4) |
|---|---|---|---|---|---|---|---|
| 2003 | VV | 19000 | 80.3±1.3±1.6 | 89± 92±31 | 139±124±27 | −90±137±42 | −55±152±42 |
| 2004 | VV | 74000 | 44.2±0.4±1.5 | 74± 80±17 | 171±103±15 | −14±131±30 | −58±146±30 |
| 2006 | VV | 312000 | 80.0±1.0±1.5 | 94± 35±10 | 97± 35±10 | −13± 48±10 | −36± 48±12 |
| 2006 | V | 111000 | 80.0±1.0±1.5 | | | −50± 55±21 | |
| 2007 | VV | 1747000 | 77.4±0.2±0.7 | 59± 13± 5 | 63± 14± 5 | 13± 18± 6 | −5± 18± 6 |
| 2007 | V | 711000 | 77.4±0.2±0.7 | | | 9± 20±13 | |
| Total | | 2974000 | | 64± 12± 4 | 69± 13± 4 | 5± 13± 5 | −10± 17± 5 |

The detailed comparison of both methods is still underway.

In Figure 4(a, b), the new results have been included in the exclusion plots involving all experimental information available from nuclear and neutron beta decays as surveyed in Ref. [6]. These are the updated exclusion plots

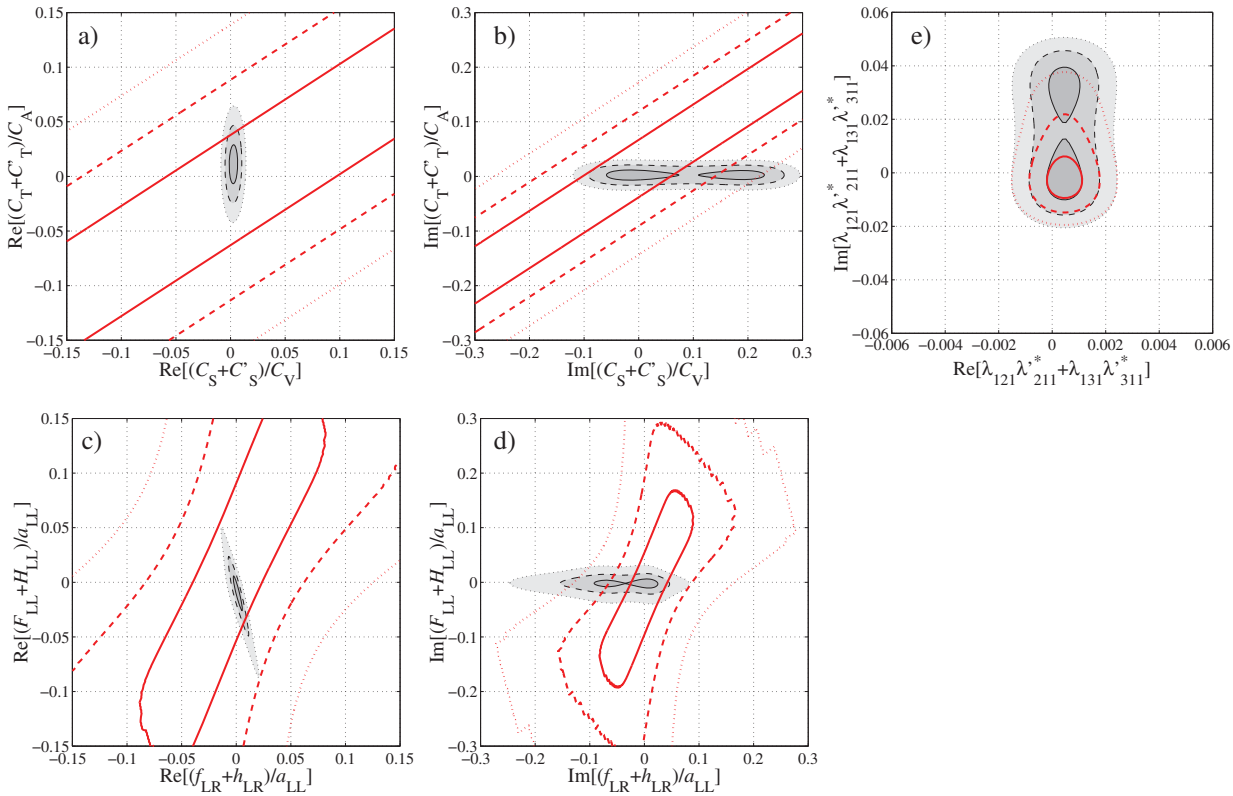


Figure 4: Experimental bounds on the scalar vs. tensor normalized couplings (panels a, b) and leptoquark exchange helicity projection amplitudes (panels c, d). The gray areas represent the information as defined in Ref. [6], while the red lines represent the limits resulting from the present experiment. Solid, dashed and dotted lines correspond to 1-, 2- and 3- sigma confidence levels, respectively, in analogy to decreasing intensity of the grey areas. Panel e: experimental bounds on the MSSM RPV coupling constant combination $\lambda_{121}\lambda'^{*}_{211} + \lambda_{131}\lambda'^{*}_{311}$.

published in Ref. [4]. The panels a) and b) contain the normalized coupling constants $\mathfrak{S}$ and $\mathfrak{T}$ defined as:

$$\mathfrak{S} \equiv \frac{C_S + C'_S}{C_V}, \qquad \mathfrak{T} \equiv \frac{C_T + C'_T}{C_A}. \tag{5}$$

The panels c) and d) correspond to the helicity projection amplitudes in the leptoquark exchange model, as defined in Ref. [7].

In the minimal super-symmetric models (MSSM), the $R$-parity violating term due to the selectron exchange generates a scalar contribution which can be traced in the nuclear and neutron beta decay as a nonzero value of the coupling constant $C_S$. According to Ref. [8] $C_S$ can be expressed as a combination of the model coupling constants $\lambda_{ijk}$, $\lambda'_{ijk}$, masses of the exchanged particles $m_{\tilde{e}_L} \approx 100$ GeV and $g_S$ which is related to the neutron, proton and light quark masses:

$$C_S = g_S \left( \frac{\lambda_{121}\lambda'^{*}_{211}}{4m^2_{\tilde{e}_{L2}}} + \frac{\lambda_{131}\lambda'^{*}_{311}}{4m^2_{\tilde{e}_{L3}}} \right), \qquad g_S = \frac{M_n - M_p}{m_d - m_u} = 0.49 \pm 0.17. \tag{6}$$

The presently best direct constraint for the imaginary part of the scalar interaction obtained in the reported experiment can be translated to the limits of the coupling constant combination $\lambda_{121}\lambda'^{*}_{211} + \lambda_{131}\lambda'^{*}_{311}$ as presented in the exclusion

plot in Fig. 4(e). The limits for the real part of $C_S$ were adopted from the compilation of the superallowed Fermi nuclear beta decays [9].

## 3. Transverse electron polarization in neutron decay

After successful completion of the pioneering experiment measuring the transverse polarization of electrons emitted in the neutron decay the following questions arise: (i) Is this quantity of further interest from the theoretical point of view? (ii) What experimental accuracy can be realistically achieved (provided, of course, that the answer for the first question is positive)? Generally, in the Standard Model, the electrons emitted in beta decay are longitudinally polarized which reflects the parity violating V-A structure of the weak interaction. The departure of the polarization vector from a strict collinearity with electron momentum can be caused by electromagnetic effects, recoil order corrections (induced couplings) or genuine scalar and tensor interactions. Thus, provided that the electromagnetic and recoil order corrections are under control, the transverse electron polarization is an ideal observable for searches of physics beyond the Standard Model. The additional advantage of the neutron decay is that it is a mixed transition so the genuine scalar and tensor couplings are available at once. Simultaneously, the uncertainty of the Fermi and Gamow-Teller matrix elements is negligible.

The transverse electron polarization is reflected in the distribution of the decay products via a number of the correlation coefficients relating it to other vectors characterizing the system, the most important being the electron and antineutrino momenta $\mathbf{p}_e$, $\mathbf{p}_{\bar{\nu}}$ and the neutron spin $\mathbf{J}$. The corresponding formula limited to the lowest order terms can be found in the classical papers [10, 11, 12]. Dropping out all the terms not depending explicitly on the transverse components of the electron polarization and retaining five exceptions ($a$, $b$, $A$, $B$ and $D$) for the reason which will become clear later, one arrives at:

$$\begin{aligned}\omega(E_e,\Omega_e,\Omega_{\bar{\nu}}) \;\propto\;& 1 + a\,\frac{\mathbf{p}_e\cdot\mathbf{p}_{\bar{\nu}}}{E_eE_{\bar{\nu}}} + b\,\frac{m_e}{E_e} + \frac{\langle\mathbf{J}\rangle}{J}\cdot\left[A\,\frac{\mathbf{p}_e}{E_e} + B\,\frac{\mathbf{p}_{\bar{\nu}}}{E_{\bar{\nu}}} + D\,\frac{\mathbf{p}_e\times\mathbf{p}_{\bar{\nu}}}{E_eE_{\bar{\nu}}}\right] \\ &+ \boldsymbol{\sigma}_\perp\cdot\left[H\,\frac{\mathbf{p}_{\bar{\nu}}}{E_{\bar{\nu}}} + L\,\frac{\mathbf{p}_e\times\mathbf{p}_{\bar{\nu}}}{E_eE_{\bar{\nu}}} + N\,\frac{\langle\mathbf{J}\rangle}{J} + R\,\frac{\langle\mathbf{J}\rangle\times\mathbf{p}_e}{J\,E_e} + S\,\frac{\langle\mathbf{J}\rangle}{J}\frac{\mathbf{p}_e\cdot\mathbf{p}_{\bar{\nu}}}{E_eE_{\bar{\nu}}} + U\,\mathbf{p}_{\bar{\nu}}\frac{\langle\mathbf{J}\rangle\cdot\mathbf{p}_e}{J\,E_eE_{\bar{\nu}}} + V\,\frac{\mathbf{p}_{\bar{\nu}}\times\langle\mathbf{J}\rangle}{J\,E_{\bar{\nu}}}\right],\end{aligned} \tag{7}$$

where $\boldsymbol{\sigma}_\perp$ represents a unit vector perpendicular to the electron momentum $\mathbf{p}_e$ and $J = |\mathbf{J}|$. In the infinite neutron mass approximation (no recoil), making usual assumptions for the Standard Model: $C_V = C'_V = 1$ and $\lambda \equiv C_A = C'_A = -1.2694$ [5], and neglecting the contributions quadratic (and higher order) in $C_S, C'_S, C_T, C'_T$ one can express all the correlation coefficients from Eq. (7) (called here $X$) as linear combinations of the real and imaginary parts of $\mathfrak{S}$ and $\mathfrak{T}$ defined in Eq. (5):

$$X = X_{\mathrm{SM}} + X_{\mathrm{FSI}} + c_{\mathrm{Re}S}\,\Re(\mathfrak{S}) + c_{\mathrm{Re}T}\,\Re(\mathfrak{T}) + c_{\mathrm{Im}S}\,\Im(\mathfrak{S}) + c_{\mathrm{Im}T}\,\Im(\mathfrak{T}). \tag{8}$$

The coefficients in this expression are functions of $\lambda$ and kinematical quantities. Table 2 summarizes their values calculated with the kinematical factors averaged over the electron spectrum in the kinetic energy range 200–783 keV. $X_{\mathrm{SM}}$ is the SM value of $X$ and the electromagnetic corrections called $X_{\mathrm{FSI}}$ were calculated in the static Coulomb field approximation with point-like proton and including only the contributions linear in the fine structure constant $\alpha$ [11, 12].

The coefficients $H$ through $V$ relating the transverse electron polarization to $\mathbf{p}_e$, $\mathbf{p}_{\bar{\nu}}$ and $\mathbf{J}$ have several interesting features. They vanish in the SM what is advantageous in searches for physics beyond the SM. They reveal variable size of the FSI contributions, from very small to easily measurable in the present experiments. This opens up a new testing ground for a systematic study of such effects. And, last but not least, the dependence on real and imaginary parts of the scalar and tensor couplings alternates exclusively from one correlation coefficient to another with varying linear combination coefficients. This feature allows one to deduce a complete set of constraints for $\mathfrak{S}$ and $\mathfrak{T}$ from the neutron decay alone. Figure 5 shows the expected constraints imposed by the $H$ through $V$ coefficients measured with an accuracy of $5\times10^{-4}$ compared to the present information combined from both neutron and nuclear beta decays.

## 4. Next generation experiment

The experiment reported in Section 2 has clearly proven that the transverse electron polarization of electrons emitted in the decay of cold neutrons can be accurately measured with Mott scattering polarimetry. The applied technique

Table 2: Coefficients defined in Eq. (8). Exceptions are the values in brackets corresponding to $(|C_S|^2 + |C'_S|^2)/2$ and $(|C_T|^2 + |C'_T|^2)/2$, respectively, the terms frequently used in the electron-neutrino correlation experiments.

| $X$ | $X_{\mathrm{SM}}$ | $X_{\mathrm{FSI}}$ | $c_{\mathrm{Re}S}$ | $c_{\mathrm{Re}T}$ | $c_{\mathrm{Im}S}$ | $c_{\mathrm{Im}T}$ |
|---|---|---|---|---|---|---|
| $a$ | −0.104793 | 0 | (−0.171405) | (+0.171405) | −0.000727 | +0.001171 |
| $b$ | 0 | 0 | +0.171405 | +0.828595 | 0 | 0 |
| $A$ | −0.117233 | 0 | 0 | 0 | −0.000923 | +0.001420 |
| $B$ | +0.987560 | 0 | −0.126422 | +0.194539 | 0 | 0 |
| $D$ | 0 | 0 | 0 | 0 | +0.000923 | −0.000923 |
| $H$ | 0 | +0.060888 | −0.171405 | +0.276198 | 0 | 0 |
| $L$ | 0 | −0.000444 | 0 | 0 | +0.171405 | −0.276198 |
| $N$ | 0 | +0.068116 | −0.217582 | +0.334815 | 0 | 0 |
| $R$ | 0 | +0.000497 | 0 | 0 | −0.217582 | +0.334815 |
| $S$ | 0 | −0.001845 | +0.217582 | −0.217582 | 0 | 0 |
| $U$ | 0 | 0 | −0.217582 | +0.217582 | 0 | 0 |
| $V$ | 0 | 0 | 0 | 0 | −0.217582 | +0.217582 |

of electron tracking and reconstruction of the scattering vertices is a powerful tool for reduction of background typical in experiments with intense neutron beams. The rich experience and quantitative information gained in that pioneering experiment allow for a realistic planning of the next steps. The main factors limiting the achieved accuracy were: (i) small angular coverage of the detecting system, (ii) relatively weak, divergent and poorly polarized cold neutron beam as compared to present possibilities and (iii) transport of neutrons in helium gas which allowed for simple and very thin ($\approx$2.5 $\mu$m Mylar) detector windows but, simultaneously, contributed significantly to the background increase (about 3% of beam neutrons scattered from helium were captured in detectors and surroundings). The idea described in the following incorporates not only the conclusions from the first experiment but implements new features which make the proposed experimental setup more universal.

The proposed experiment will measure 11 correlation coefficients ($a$, $A$, $B$, $D$, $H$, $L$, $N$, $R$, $S$, $T$, $U$, $V$) as compared to three ($A$, $N$, $R$) accessible in the former setup. We plan to optimize the proposed experiment towards the transverse electron polarization related coefficients. It is not our immediate goal to compete with specialized projects addressing the coefficients $a$, $b$, $A$, $B$ and $D$ [15–22]. Obviously, the simultaneous measurements of these will help us to keep systematics under control. In further perspective, they can become stand alone results. This, in turn, can be very intriguing since our experimental technique is completely different from that applied in the above mentioned specialized experiments. Also different are the associated systematic effects.

The strategy of the proposed experiment is to reconstruct event-by-event the decay kinematics together with the decay origin and, in this way, reduce the effects due to the large size of the decay source. In particular, fixing the three-body decay kinematics by the measured electron energy and relative $e - p$ angle one realizes that the proton energy and thus the proton time-of-flight must choose between two discrete (and known) values (see Fig. 6). The measurement of momenta of electrons and protons in coincidence allows to reconstruct the antineutrino momentum and accesses the terms dependent on this quantity.

The key ideas of the proposed setup are:

1. Efficient cylindrical detector geometry.
2. Electron tracking in a multi-wire drift chamber (MWDC) with both wire ends readout.
3. Detection of both direct and Mott-scattered electrons in a plastic scintillator hodoscope.
4. Conversion of protons (accelerated to 20-30 keV) into bunches of electrons ejected from a thin LiF layer.
5. Acceleration and subsequent detection of ejected electrons in a multi-wire proportional chamber (MWPC) with both wire ends readout.

The cylindrical geometry was already considered in the context of the $R$ correlation coefficient measurement [13] but not attempted as too challenging for a pioneering experiment. The detection of recoil protons in conjunction with electron tracking is the new feature.

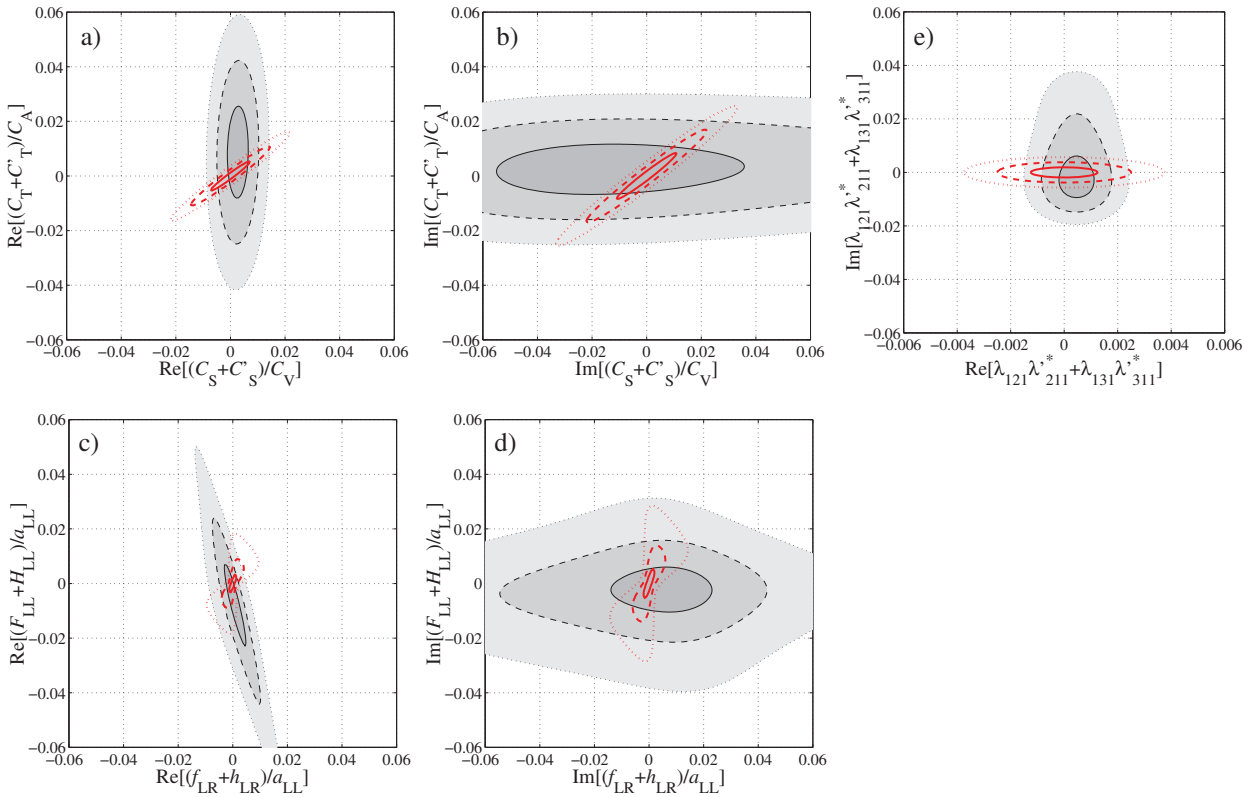


Figure 5: Expected bounds on the scalar vs. tensor normalized couplings (panels a, b), the leptoquark exchange helicity projection amplitudes (panels c, d) and the RPV MSSM coupling constants combination (panel e) from the correlation coefficients $H$, $L$, $N$, $R$, $S$, $U$ and $V$ measured with the anticipated accuracy of $5 \times 10^{-4}$. The meaning of shading and lines is the same as in Fig. 4.

A cross section of the proposed cylindrical Mott polarimeter is sketched in Fig. 7(a). The cold neutron beam is either not polarized or polarized longitudinally. The vacuum of the decay volume is separated from gas detectors with a 6 $\mu$m thick Mylar foil supported by a light but rigid mesh-like cylindrical structure. The gas detector consists of a single layer MWPC followed by a five layer MWDC. MWPC has the gain adjusted such that it is sensitive to only large signals of multiple 20-30 keV electrons produced in a 100 nm thick $p - e$ conversion foil [14]. The penetration depth of these electrons in gas is of the order of 1 cm so they do not reach the MWDC. Decay electrons are tracked in MWDC and reach the Mott target made of 1-2 $\mu$m thick lead (or depleted uranium) layer deposited on a thin Mylar substrate. The decay electrons can be either backscattered (about 1 in 1000 cases) or pass the foil and be detected in a plastic scintillator hodoscope located close to it. The Mott-scattered electrons are also registered in a hodoscope. The expected average (optical) transparency of the vacuum window is about 80% so the maximum loss factor (three passes through windows by Mott-scattered electrons) is about 2 and feasible energy threshold ≈200 keV. For the direct electrons and protons the feasible losses are of the order of 20% and corresponding energy thresholds of 100 keV and 100 eV, respectively.

The key features of the data acquisition will be:

1. Only one trigger condition – registration of an electron in the plastic scintillator hodoscope. This signal will also be a time reference for all other signals appearing on MWDC and MWPC.
2. Acquisition of all signals appearing on wires within a time window of about 1 $\mu$s.
3. Wave form digitization of all signals with 1 ns resolution.
4. Deduce: (i) electron energy from pulse height in the scintillator, (ii) proton hit position from pulse height asymmetry on both wire ends in MWPC, (iii) proton time-of-flight, (iv) electron track from drift times and pulse height asymmetry on both wire ends in MWDC.

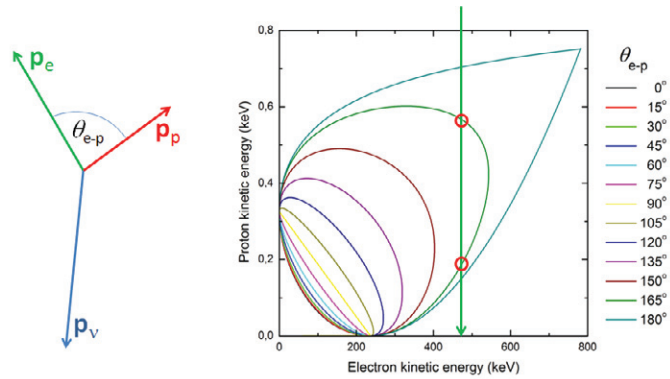


Figure 6: Three-body kinematics of the ordinary neutron decay. For fixed relative electron-proton angle $\theta_{e-p}$ and electron energy one is left with (at most) two discrete solutions for proton energy.

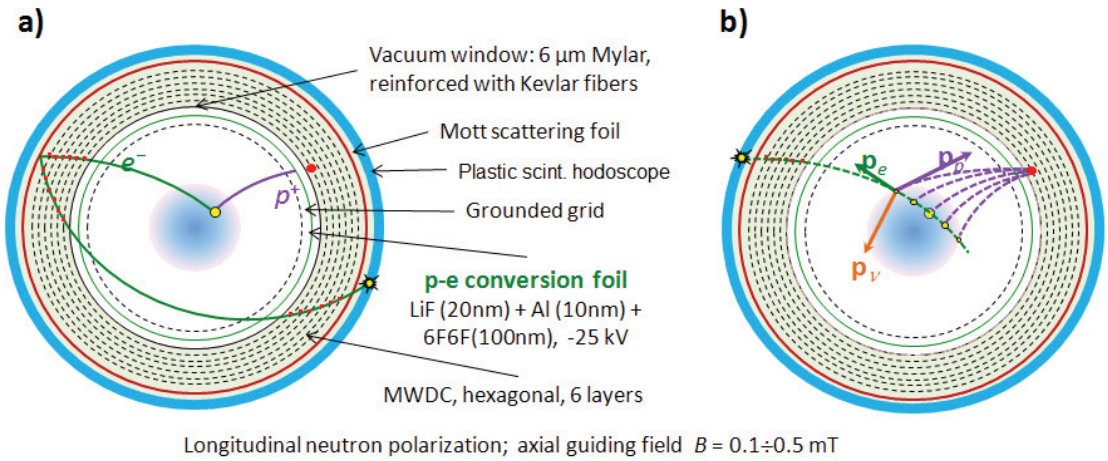


Figure 7: a) Sketch of the proposed experimental setup in the cylindrical geometry. Only the cross section perpendicular to the detector axis is shown. b) Conditional reconstruction of 3-body decay kinematics. The sizes of the yellow dots represent the probabilities assigned to particular solutions.

The proposed solutions imply an unbiased registration of direct electrons (without Mott scattering) and also without accompanying protons. Fixed 3-body decay kinematics and thus fixed relation between electron energy and proton time-of-flight will allow for a short coincidence time window which reduces significantly accidental coincidences and allows for large single rates of detectors. On the other hand, the fine granularity of the proposed detecting system (5 mm pitch for MWPC and 10 mm for MWDC) guaranties that even an outstanding neutron decay rate of $10^5$ s$^{-1}$ in the fiducial volume will cause the pulse rate of less than 1 kHz on a 2 m long wire.

Although, due to the finite size of the beam cross section, the exclusive kinematics can be reconstructed only approximately, the gain of information over the classical "integral" approach to cope with an extended decay source is significant. Conditional reconstruction of the decay vertex and thus the proton and antineutrino momenta with precisely known weights (decay probability distribution along the reconstructed electron path segment coinciding with the beam is known, cf. Fig. 7(a)) is sufficient since for the extraction of the correlation coefficients one must anyhow integrate over momenta.

The experiment can be run in two modes: (1) unpolarized neutrons – measurement of $a$, $H$, $L$ and (2) polarized neutrons – measurement of $a$, $A$, $B$, $D$, $H$, $L$, $N$, $R$, $S$, $U$ and $V$ coefficients. In the extraction of the correlation

coefficients, the symmetry properties of particular terms with respect to the transformations $\mathbf{J} \to -\mathbf{J}$, $\mathbf{p}_e \to -\mathbf{p}_e$ and $\mathbf{p}_{\bar{\nu}} \to -\mathbf{p}_{\bar{\nu}}$ will be utilized. It has been estimated that with a 2 m long detecting system, $10^5$ decays per second in the fiducial volume and three month long data taking period one can acquire:

1. $3 \times 10^8$ Mott-scattered electrons (coefficients $N$, $R$),
2. $10^8$ protons in coincidence with Mott-scattered electrons (coefficients $H$, $L$, $S$, $U$, $V$),
3. $10^{12}$ direct electrons (coefficient $A$),
4. $3 \times 10^{11}$ protons in coincidence with direct electrons (coefficients $a$, $B$, $D$).

These numbers are sufficient for the anticipated sensitivity of about $5 \times 10^{-4}$ for the transverse electron polarization related correlation coefficients.

## 5. Summary

In the pioneering experiment, two components of the transverse polarization of electrons emitted in the neutron decay were successfully measured with the statistical accuracy of about 0.012 and two times smaller systematical uncertainty. The results agree with the Standard Model and allowed to tighten the experimental constraints on the imaginary part of the linear combination of the scalar and tensor contributions to the vector and axial vector interactions dominating in beta decay. This, in turn, improved the constraints on the exotic contributions from the leptoquark exchange and $R$ parity violating MSSM processes. The success of the applied Mott polarimetry and electron tracking technique allows for realistic planning of a future experiment with the goal to measure and explore the transverse electron polarization with the accuracy better than $5 \times 10^{-4}$.

## Acknowledgments

This work was supported in part by Polish Committee for Scientific Research under the Grant No. 2P03B11122, the Fund for Scientific Research Flanders (FWO) and the project GOA/2004/03 of the K.U.Leuven.' and by an Integrated Action Program Polonium (Contract No. 05843UJ). Part of the computation work was performed at ACK Cyfronet, Krakow. The collaboration is grateful to PSI for excellent support and kind hospitality. One of the authors (KB) would like to thank W.M. Snow, University of Indiana, Bloomington, IN, USA, for stimulating discussions.

## References

[1] G. Ban et al., Nucl. Instrum. Methods Phys. Res., Sect. **A 565**, 711 (2006).
[2] A. Gellrich, J. Kessler, Phys. Rev. **A 43**, 204 (1991).
[3] J. Sromicki et al., Phys. Rev. Lett. **92**, 57 (1999).
[4] A. Kozela et al., Phys. Rev. Lett. **102**, 172301 (2009).
[5] K. Nakamura et al. (Particle Data Group), J. Phys. **G 37**, 075021 (2010).
[6] N. Severijns et al., Rev. Mod. Phys. **A 78**, 991 (2006).
[7] P. Herczeg, Prog. Part. Nucl. Phys. **46**, 413 (2001).
[8] N. Yamanaka et al., J. Phys. G: Nucl. Part. Phys. **37**, 055104 (2009).
[9] J.C. Hardy and I.S. Towner, Phys. Rev. **C 79**, 055502 (2009).
[10] J. Jackson, S. Treiman and H. Wyld, Phys. Rev. **106**, 517 (1957).
[11] J. Jackson, S. Treiman and H. Wyld, Nucl. Phys. **4**, 206 (1957).
[12] M. E. Ebel and G. Feldman, Nucl. Phys. **4**, 213, (1957).
[13] J. Sromicki, Nucl. Instr. Meth. Phys. Res. **A 440**, 609 (2000).
[14] S. Hoedl et al., J. Appl. Phys. **99**, 084904 (2006).
[15] W. S. Wilburn et al., J. Res. NIST **110**, 389 (2005).
[16] B. Maerkisch et al., Nucl. Instr. Meth. Phys. Res. **A 611**, 216 (2009).
[17] D. Dubbers et al., Nucl. Instr. Meth. Phys. Res. **A 596**, 238 (2008).
[18] O. Zimmer et al., Nucl. Instr. Meth. Phys. Res. **A 440**, 548 (2000).
[19] F.E. Wietfeldt et al., Nucl. Instr. Meth. Phys. Res. **A 611**, 207 (2009).
[20] B. Tipton et al., AIP Conf. Proc. **539**, 286 (2000).
[21] R. Alarcon et al., Letter of intent, http://nab.phys.virginia.edu/nab_loi.pdf
[22] H.P. Mumm et al., Rev. Sci. Instr. **75**, 5343 (2004).